JOURNAL OF GEOPHYSICAL RESEARCH, VOL. 106, NO. C1, PAGES 1085–1096, JANUARY 15, 2001

Two-phase, near-field modeling of purposefully released CO_2 in the ocean

Guttorm Alendal and Helge Drange

Nansen Environmental and Remote Sensing Center, Bergen, Norway

Abstract. Injection of carbon dioxide (CO_2) in the ocean has been proposed as an option for accelerating the natural net flux of CO_2 from the atmosphere into the ocean. Liquid CO_2 released as droplets at depths <3000 m will create an ascending plume of droplets and entrained water. As the CO_2 droplets dissolve, carbon is transferred into the plume water, yielding increased density and a lowered pH value of the plume water. As ambient water entrains the CO_2-enriched water by mixing, the density difference disappears and the injected CO_2 follows the ocean dynamics as a dynamically passive tracer. Here we report on numerical experiments performed with a two-phase Navier Stokes solver. The effects of different droplets sizes, background currents, and injection rates are examined. The numerical experiments show that the droplet size and the background current are key parameter for predicting the vertical distribution of the plume water, the associated reduction in the pH field, and the increase in the plume water density. If rapid dilution of the CO_2-enriched water is the objective (leading to modest reduction in the pH value), large initial droplets and high background currents are preferable. On the other hand, if the objective is to increase the density of the plume water in order to generate a sinking plume (yielding enhanced residence time of the released CO_2), CO_2 injection with small droplets in a stagnant water column is optimal.

1. Introduction

The atmospheric concentration of carbon dioxide, the principal human-induced greenhouse gas, has increased from ~280 parts per million (ppm) (or 0.028%) at the beginning of the Industrial Revolution to ~365 ppm today. This increase is mainly caused by burning of oil, coal, and gas and changes in the use of land. An increasing human population, increased standard of living in the developing parts of the world, no apparent alternative large-scale energy substitute except for nuclear energy, and a known recoverable fossil fuel reserve of 3000–5000 Gt C indicate that the man-made emissions of CO_2 will double over the next century and that the fossil fuel era may last for several generations (see, for example, *Schimel et al.* [1996] for a description of CO_2 and the carbon cycle).

The world ocean waters and calcareous ($CaCO_3$) ocean sediments are able to absorb all but a few per cent of the CO_2 released to the atmosphere [*Broecker and Peng*, 1982], if the known global fossil fuel reserve is utilized by conventional combustion schemes. For the present-day situation, about one third of the annual fossil fuel CO_2 emissions of ~5.5 Gt C are absorbed by the ocean surface waters over 3-5 years. Unfortunately, the huge chemical absorption capacity of the marine environment is heavily rate limited by the long (>1000 years) physical mixing timescale between the world ocean surface, intermediate and deep waters, and the subsequent dissolution of sedimentary $CaCO_3$.

It was therefore proposed by *Marchetti* [1977] to accelerate the natural ocean uptake of atmospheric CO_2 by collecting the gas from point sources and by releasing it into the ocean at appropriate locations and at depths sufficient to avoid direct outgassing to the atmosphere. Marchetti identified the Strait of Gibraltar as a promising place; here the saline and dense outflowing Mediterranean water sinks to ~1000 m before it spreads out over large parts of the Atlantic basin.

Marchetti [1977] was followed by *Hoffert et al.* [1979], who used a simple, horizontally integrated box model and examined the atmospheric response of ocean disposal of CO_2. The model calculations are based on emission rates that are rather extreme (7000 Gt C released between year 1900 and year 2200), but the results illustrate the effect of ocean disposal of CO_2: By injecting CO_2 into the ocean, one can reduce the transient peak in the atmospheric CO_2 concentration. This result was later confirmed in similar studies [*Sundquist*, 1986; *Wilson*, 1992] and by using global three-dimensional ocean circulation carbon cycle models [*Bacastow and*

Paper number 1999JC000290.
0148-0227/01/1999JC000290$09.00

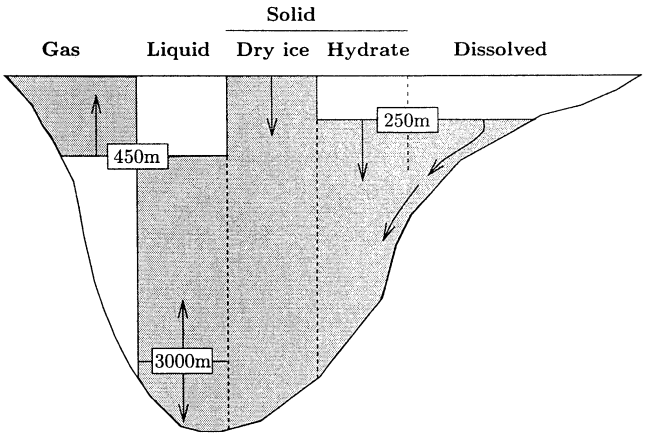

Figure 1. Overview of the different ocean disposal options. The arrows indicate the depth interval in which CO_2 in gaseous, liquid, dissolved, or solid form will ascend or descend in the water column.

Stegen, 1991; *Maier-Reimer*, 1991; *Stegen et al.*, 1993].

Several ocean disposal options exist, and the different options are closely connected to the phase properties of CO_2 for the temperature and pressure regimes encountered in the ocean and to the density of gaseous, liquid, and solid CO_2 compared to the density of seawater (see Figure 1).

Liquid CO_2 is more (less) dense than seawater at an ocean depth of ~3000 m or more (less) [*Ely et al.*, 1989] , the density of dry ice is ~1550 kg m^{-3} [*Nakashiki et al.*, 1991], and the density of pure CO_2 hydrate is ~1110 kg m^{-3} [*Golomb et al.*, 1992]. It is therefore possible to dispose of fossil fuel CO_2 in various ways: Blocks (or cylinders) of solid CO_2 will descend quickly through the water column [*Nakashiki et al.*, 1991], "lakes" of liquid CO_2 will be formed if liquid CO_2 is released on the seabed at depths of 3000 m or more [*Ohsumi*, 1993; *Shindo et al.*, 1993], and hydrates will accumulate on the ocean bottom [*Saji et al.*, 1992; *Golomb et al.*, 1992; *Brewer et al.*, 1999] .

In addition, if liquid CO_2 is released between the condensation depth (at ~450 m) and a depth of ~3000 m, droplets of liquid CO_2 will ascend through the water column and partly or fully dissolve in the surrounding water masses because of the large CO_2 concentration difference between the CO_2 particles and ambient seawater [*Herzog et al.*, 1991; *Liro et al.*, 1992; *Haugan and Drange*, 1992] . If the droplets of liquid CO_2 reach the condensation depth or if CO_2 is injected at depths shallower than the condensation depth, bubbles of CO_2 will be formed [*Herzog et al.*, 1991; *Haugan and Drange*, 1992] .

In addition, the density of seawater increases as CO_2 is dissolved in the water [*Bradshaw*, 1973], and the increase in density may exceed 10 kg m^{-3} [*Drange and Haugan*, 1992a]. An additional option is therefore to dissolve fossil fuel CO_2 in seawater (in a chamber, for instance [*Adams et al.*, 1995]) and release the dense, CO_2-enriched water on a sloping ocean bottom; thereby creating a bottom gravity current that will transport the carbon to greater depths [*Haugan and Drange*, 1992; *Drange and Haugan*, 1992a; *Drange et al.*, 1993]. Special care has to be taken so that the generated bottom-attached gravity current does not move at a constant depth in geostrophic balance [*Alendal et al.*, 1994], for instance, by releasing the CO_2-enriched water in a canyon [*Adams and Herzog*, 1997].

The rising plume resulting from releasing liquid CO_2 at depths >450 m has so far been modeled by simple steady state, one-dimensional bulk models [*Liro et al.*, 1992; *Drange and Haugan*, 1992b; *Thorkildsen and Haugan*, 1993; *Thorkildsen et al.*, 1994], where the plume consisting of CO_2 droplets and entrained water is described by horizontal averages. As a result of diffusion and subsequent dispersion of CO_2 molecules in seawater, the buoyancy of the droplets decreases. Once the negative (downward) buoyancy of the plume water exceeds the positive buoyancy of the droplets, the plume will descend in the water column. To account for this effect, the plume models perform so-called peeling events in which fractions of the dense plume water are ejected from the plume. The ejected water tends to sink in the water column, but this motion cannot be easily described by the integrated bulk models.

In a first attempt to model the behavior of the peeled off water, *Thorkildsen and Alendal* [1997] modeled the droplet plume by introducing sources of CO_2 and buoyancy into a three-dimensional nonhydrostatic Navier Stokes solver [*Alendal*, 1996]. In this simulation, results from a steady state, bulk droplet plume model [*Thorkildsen and Haugan*, 1993] were used as input to the Navier Stokes solver. The objective of the present study is to simulate the combined effect of rising droplets and of sinking, dense, CO_2-enriched seawater. The droplets have been treated as a separate phase in a Navier Stokes solver, interacting with seawater through mass transfer and interfacial drag.

Increased CO_2 concentration in seawater reduces the pH value with possible impact on the marine biota (Figure 2). The reason for this is that the species composition of the carbonic acid system in seawater changes (reduced pH and carbonate ion CO_3^{2-} concentration and increased concentration of dissolved CO_2) as the concentration of total dissolved inorganic carbon (C_T) increases [*Stumm and Morgan*, 1981]. The change in the chemistry of seawater, together with the effective exposure time experienced by marine organisms, are key input parameters for environmental studies [*Auerbach et al.*, 1997; *Caulfield et al.*, 1997]. Hence near-field diffusion and dispersion modeling studies such as the one presented here are required to assess effects on the marine biota in the vicinity of the injection site. In addition, near-field modeling of the released CO_2 will give concentration fields that can be used as a source function for simulating the behavior of CO_2 at spatial and temporal scales exceeding the scales simulated here.

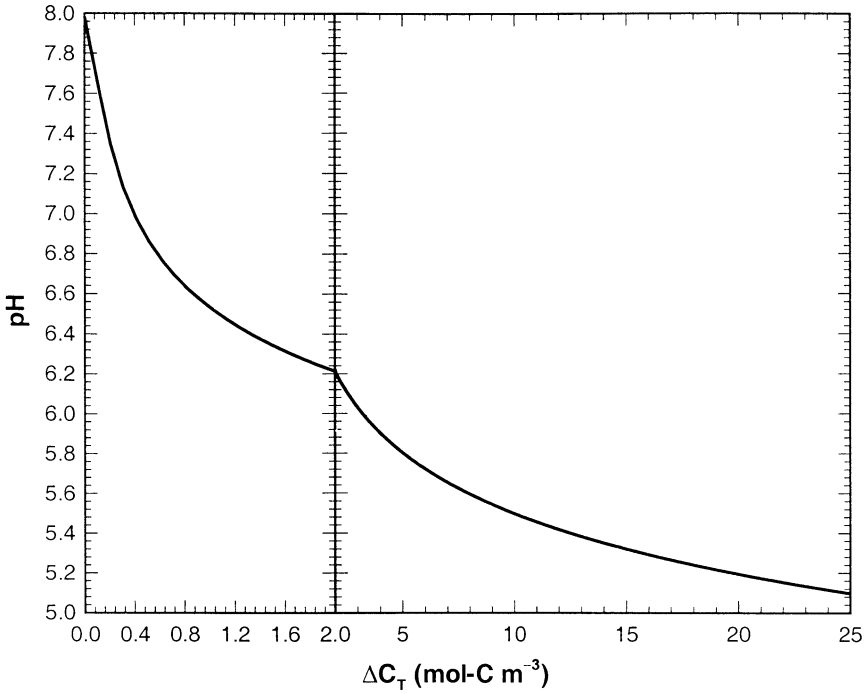

Figure 2. Computed pH value [*Drange and Haugan*, 1992a] as CO_2 is dissolved in seawater at a pressure of 35 bar and a temperature of 8°C. Here ΔC_T (mol C m^{-3}) denotes the amount of carbon added to seawater. Natural seawater has a pH value of ~8, and it contains ~2 mol C m^{-3}, so $\Delta C_T = 2$ mol C m^{-3} represents a doubling of the amount of dissolved inorganic carbon in seawater. The pH value of small values of ΔC_T has been enhanced by the use of different linear scalings of the abscissa.

The paper is outlined as follows. In section 2 the two-phase droplet model is described. Results of a set of numerical experiments are presented in section 3, followed by discussion in section 4, and conclusions in section 5.

2. Two-Phase Model

Hereafter seawater will be denoted the carrier or continuous phase (subscript c), while the CO_2 droplets will be named the dispersed phase (subscript d). The model originates from the two-phase continuum flow model of *Crowe et al.* [1998], where each phase is described by continuity and momentum equations. The carrier phase has in addition, tracer (or concentration) equations for temperature T (Kelvins), salinity S (psu), and total dissolved inorganic carbon C_T (mol C m^{-3}). A number density equation is used to close the system of differential equations.

The two phases are described by the following definitions: The number density n (m^{-3}) is given by

$$n = \lim_{\partial V \to \partial V_0} \frac{\partial N}{\partial V}, \tag{1}$$

where ∂N (no unit) is the number of elements in the volume ∂V (m^3), while ∂V_0 (m^3) is the limiting volume that assures a stationary average. The volume fraction α_d (no unit) is defined as

$$\alpha_d = \lim_{\partial V \to \partial V_0} \frac{\partial V_d}{\partial V}, \tag{2}$$

where ∂V_d (m^3) is the volume of the dispersed phase in the control volume. For the continuous phase the volume fraction α_c (no unit) , also called the void fraction, is given by

$$\alpha_c = \lim_{\partial V \to \partial V_0} \frac{\partial V_c}{\partial V}. \tag{3}$$

The relationship

$$\alpha_d + \alpha_c = 1 \tag{4}$$

ensures consistency.

In this work all droplets are assumed to be of the same size with a volume V_d (m^3) in each control volume, hence $\partial V_d = \partial N\, V_d$, and

$$\alpha_d = \lim_{\partial V \to \partial V_0} \frac{\partial N\ V_d}{\partial V} = n V_d. \tag{5}$$

Finally, the bulk or apparent density $\overline{\rho_d}$ (kg m^{-3}) is

$$\overline{\rho_d} = \lim_{\partial V \to \partial V_0} \frac{\partial M_d}{\partial V}, \tag{6}$$

where ∂M_d (kg) is the mass of the dispersed phase in the control volume. A similar definition holds for the bulk density of the continuous phase, $\overline{\rho_c}$.

If all particles have the same mass m_d (kg), then

$$\overline{\rho_d} = n m_d = \alpha_d \rho_d \,, \tag{7}$$

where ρ_d ($kg\,m^{-3}$) is the density of the droplet fluid.

2.1. Carrier Phase

According to *Crowe et al.* [1998], a continuity equation,

$$\frac{\partial}{\partial t}\alpha_c\rho_c + \nabla\cdot\alpha_c\rho_c\mathbf{u} = -s_{\text{mass}} \,, \tag{8}$$

and the momentum equations,

$$\begin{aligned}\frac{\partial}{\partial t}\alpha_c\rho_c\mathbf{u} + \nabla\cdot\alpha_c\rho_c\mathbf{u}\mathbf{u} = -\alpha_c\nabla p + \alpha_c\rho_c\mathbf{g} \\ +\alpha_c\nabla\cdot\tilde{\tau} - \beta_V(\mathbf{u}-\mathbf{v}) - \mathbf{v}s_{\text{mass}} \,,\end{aligned} \tag{9}$$

are solved for the carrier phase. Here $\mathbf{u}$ (m s^{-1}) is the three-dimensional velocity vector, ρ_c (kg m^{-3}) is the carrier phase density, $\mathbf{g}$ (m s^{-2}) is the gravitational vector, $\tilde{\tau}$ (Pa) is the stress tensor, and $s_{\text{mass}} < 0$ (kg m^{-3} s^{-1}) represents mass transfer. Furthermore, drag from the dispersed phase with velocity $\mathbf{v}$ (m s^{-1}) is proportional to the velocity difference between the two phases with a drag coefficient β_V (kg m^{-3} s^{-1}). The last term in (9) represents momentum influence on the carrier phase due to mass transfer from the dispersed phase.

Equations (8) and (9) have been recasted to fit an existing Navier Stokes solver. For this we note that the continuity equation can be put in the form

$$\frac{\partial}{\partial t}\rho_c\alpha_c + \mathbf{u}\cdot\nabla\rho_c\alpha_c + \rho_c\alpha_c\nabla\cdot\mathbf{u} = -s_{\text{mass}} \,, \tag{10}$$

or, with the definition $d/dt = \partial/\partial t + \mathbf{u}\cdot\nabla$,

$$\frac{d}{dt}\rho_c\alpha_c + \rho_c\alpha_c\nabla\cdot\mathbf{u} = -s_{\text{mass}} \,. \tag{11}$$

The change in mass for the continuous phase is given by dissolution of the dispersed phase, so

$$\frac{d}{dt}\rho_c\alpha_c = -s_{\text{mass}} \,, \tag{12}$$

yielding the ordinary, noncompressible continuity equation

$$\nabla\cdot\mathbf{u} = 0 \,. \tag{13}$$

In a similar way the momentum equation is differentiated as

$$\begin{aligned}\mathbf{u}\left(\frac{\partial}{\partial t}\overline{\rho}_c + \nabla\cdot\overline{\rho}_c\mathbf{u}\right) + \overline{\rho}_c\left(\frac{\partial}{\partial t}\mathbf{u} + \mathbf{u}\cdot\nabla\mathbf{u}\right) = \\ -\alpha_c\nabla p + \rho_c\mathbf{g} + \nabla\cdot\tilde{\tau} - \beta_V(\mathbf{u}-\mathbf{v}) - \mathbf{v}s_{\text{mass}} \,.\end{aligned} \tag{14}$$

Recognizing the continuity equation in the first term on the left-hand side and using the Boussinesq approximation, i.e., dividing through with a characteristic density ρ_0 and neglecting density variations in all terms apart from in the gravity term, yields

$$\begin{aligned}\frac{\partial}{\partial t}\mathbf{u} + \mathbf{u}\cdot\nabla\mathbf{u} = -\frac{1}{\rho_0}\nabla p' + \frac{\rho_c-\rho_0}{\rho_0}\mathbf{g} + \\ \frac{1}{\rho_0}\nabla\cdot\tilde{\tau} - \frac{\beta_V}{\rho_0\alpha_c}(\mathbf{u}-\mathbf{v}) + \frac{s_{\text{mass}}}{\rho_0\alpha_c}(\mathbf{u}-\mathbf{v}) \,.\end{aligned} \tag{15}$$

Here the pressure term has been decomposed into a hydrostatic p_0 and dynamic p' pressure term $p = p_0 + p'$, with $\nabla p_0 = \rho_0\mathbf{g}$. The last term in (15) represents the momentum influence from mass transfer, and this term has been neglected as it is small.

The tracer equations for temperature and salinity, the former by neglecting heat from the dissolution process, can be written as

$$\frac{\partial}{\partial t}T + \nabla\cdot T\mathbf{u} = \nabla\cdot\kappa_T^e\nabla T \,, \tag{16}$$

$$\frac{\partial}{\partial t}S + \nabla\cdot S\mathbf{u} = \nabla\cdot\kappa_S^e\nabla S \,, \tag{17}$$

where κ_T^e (m^2 s^{-1}) and κ_S^e (m^2 s^{-1}) are, respectively, temperature and salinity turbulent diffusivities (see below).

For carbon a source term enters the conservation equation due to dissolution of CO_2 from the droplets, so

$$\frac{\partial}{\partial t}C_T + \nabla\cdot C_T\mathbf{u} = \nabla\cdot\kappa_C^e\nabla C_T - s_{\text{mass}}/M_{CO_2} \,, \tag{18}$$

where $M_{CO_2} = 44.01\times10^{-3}$ kg (mol C)$^{-1}$ is the molar mass of CO_2.

2.2. Dispersed Phase

The continuity equation for the dispersed phase is similar to the carrier phase with reversed sign on the mass transfer term and with an additional term I_{mass} (kg m^{-3} s^{-1}) describing the injection of CO_2 droplets:

$$\frac{\partial}{\partial t}\alpha_d\rho_d + \nabla\cdot\alpha_d\rho_d\mathbf{u} = s_{\text{mass}} + I_{\text{mass}} \,. \tag{19}$$

A momentum equation for the dispersed phase can also be given, but here it is assumed that the dispersed droplets move with the carrier phase with an additional vertical terminal velocity U_T (m s^{-1}), so

$$\mathbf{v} = \mathbf{u} + U_T\mathbf{k} \,, \tag{20}$$

where $\mathbf{k}$ is a unit vector in the vertical direction.

In order to close the set of equations, a number density equation has been introduced. The rate of change of number density depends on the flux of droplets in and out of a volume and the number injected I_n (m^{-3} s^{-1}) [*Ferziger and Perić*, 1997], so

$$\frac{\partial}{\partial t}\int_{V_0} n\,d\Omega + \int_{\Gamma_0} n\mathbf{v}\nabla\cdot\mathbf{m}\,dS = \int_{V_0} I_n\,d\Omega \,. \tag{21}$$

Here V_0 (m^3) and Γ_0 (m^2) are the volume and the surface area of the control volume, respectively, and the

surface normal vector is denoted **m**. Using Gauss law on the surface integral and collecting the terms give

$$\int_{V_0} \left(\frac{\partial}{\partial t} n + \nabla \cdot n\,\mathbf{v} - I_n \right) d\Omega = 0\,. \tag{22}$$

As long as a stationary average can be reached, the control volume can be chosen arbitrary, giving the following continuity equation for the number density:

$$\frac{\partial}{\partial t} n + \nabla \cdot n\mathbf{v} = I_n\,. \tag{23}$$

2.3. Parameters

The international equation of state [*UNESCO*, 1981] has to be extended to take into account the effect that enhanced concentration of dissolved inorganic carbon has on seawater density [*Drange and Haugan*, 1992a],

$$\rho_c = \rho(S,T,p) + [M_{\mathrm{CO}_2} - \rho(S,T,p) v_{\mathrm{CO}_2}]\, C_T\,. \tag{24}$$

Here $\rho(S,T,p)$ (kg m^{-3}) is the seawater density according to the standard equation of state and $v_{\mathrm{CO}_2} = 34 \times 10^{-6}$ m^3 (mol C)$^{-1}$ is a conservative (high) estimate of the molar volume of CO_2 [*Drange and Haugan*, 1992a]. For the pressure range considered here, v_{CO_2} can be treated as constant. Furthermore, the equation of state for liquid CO_2 is given by *Ely et al.* [1989].

For the stress tensor, a Smagorinsky parameterized stress has been used with proportionality to the shear [*McComb*, 1990]:

$$\tau_{ij} = -\rho_0 \nu_e \left(\frac{\partial \overline{u}_i}{\partial x_j} + \frac{\partial \overline{u}_j}{\partial x_i} \right)\,. \tag{25}$$

Here ν_e (m^2 s^{-1}) is the local eddy viscosity, given by

$$\nu_e = c^2 \Delta^2 \tilde{\mathcal{S}}^{1/2}, \tag{26}$$

where $c = 0.079$ is a constant [*Yakhot and Orszag*, 1986], Δ is a filter width taken to be the grid spacing, and

$$\tilde{\mathcal{S}} = \frac{\partial \overline{u}_i}{\partial x_j} \left(\frac{\partial \overline{u}_i}{\partial x_j} + \frac{\partial \overline{u}_k}{\partial x_i} \right) \tag{27}$$

is the shear.

Yakhot and Orszag [1986] provide a turbulent or eddy diffusivity parameterization based on renormalization group (RNG) theory:

$$\left| \frac{\phi - 1.3929}{\phi_0 - 1.3929} \right|^{0.6321} \left| \frac{\phi + 2.3929}{\phi_0 + 2.3929} \right|^{0.3679} = \frac{\nu_0}{\nu_e}\,, \tag{28}$$

where

$$\phi = \frac{\kappa_S^e}{\nu_e}, \quad \phi_0 = \frac{\kappa_S^0}{\nu_0} \tag{29}$$

are, respectively, the turbulent and molecular inverse Schmidt numbers, in this case for salinity but similar for the other two scalars (temperature and carbon concentration). Notice if the turbulent viscosity ν_e equals the molecular viscosity ν_0 (both in m^2 s^{-1}), $\kappa_S^e = \kappa_S^0$. In the other extreme where the turbulent viscosity is much larger than the molecular viscosity, the fraction on the right-hand side of (28) approaches zero, giving a turbulent diffusivity of $\kappa_S^e = 1.3929\nu_e$. The equation involves solving a nonlinear equation for each computational node for each time step, so the solutions for (28) have been evaluated once for the range

$$0 < \frac{\nu_0}{\nu_e} \le 1 \Rightarrow \phi_0 \le \phi \le 1.3929$$

and stored in an array.

The drag coefficient has been taken from the development of the slip velocity, which assumes that the droplets move with the terminal velocity U_T (m s^{-1}) when the drag and buoyancy forces balance. The buoyancy F_G (N) on a droplet is, assuming that the gravity works in the vertical direction only,

$$F_G = V_d\, g\, (\rho_c - \rho_d)\,, \tag{30}$$

which has to balance the drag force F_D (N) on one particle given by

$$F_D = \beta_d (u - v) = \beta_d U_T. \tag{31}$$

For each particle then the drag coefficient (kg s^{-1}) is

$$\beta_d = \frac{V_d g\, (\rho_c - \rho_d)}{U_T}\,. \tag{32}$$

Summing over all the droplets in a control volume, dividing by volume, and letting the volume go to the limit volume gives the drag coefficient in (14),

$$\beta_V = \lim_{\partial \mathcal{V} \to \partial \mathcal{V}_0} \frac{\partial N V_d g\, (\rho_c - \rho_d)}{\partial\, V U_T} = \frac{\alpha_d g\, (\rho_c - \rho_d)}{U_T}\,. \tag{33}$$

According to *Cussler* [1984] , the mass transfer from one droplet with radius r (m) can be put in the form

$$\frac{d}{dt} \left(\frac{4}{3} \rho_d r^3 \right) = -4\pi r^2 K M_{\mathrm{CO}_2} (C_s - C)\,. \tag{34}$$

Here $C_s = 1360$ mol C m^{-3} and C are the concentrations of CO_2 at the droplet surface and far away from the droplets, respectively. C_s is obtained from the equation of state for liquid CO_2 [*Ely et al.*, 1989] and is treated as constant. The mass transfer coefficient K (m s^{-1}) has been taken from *Clift et al.* [1978],

$$K = \frac{2}{\sqrt{\pi}} \left(1 - \frac{2.89}{\sqrt{Re_k}} \right) \sqrt{\frac{\kappa_C^0 U_T}{2r}}\,, \tag{35}$$

where

$$Re_k = \frac{2\rho_d r U_T}{\nu_0} > 70 \tag{36}$$

is a dimensionless Reynolds number. This is the mass transfer from a single droplet, whereas the mass transfer per unit volume s_{mass} (kg m^{-3} s^{-1}) is obtained by multiplying with the number density, so

$$s_{\text{mass}} = -n4\pi r^2 K M_{CO_2}(C_s - C)\,. \quad (37)$$

The mass transfer is negative in order to keep notation according to *Crowe et al.* [1998].

A particle in stagnant fluid will be influenced by buoyancy and drag on the droplet interface. When these forces balance, the droplets move with a constant settling or slip velocity. In the present study the terminal velocity given by *Clift et al.* [1978],

$$U_T = 0.711\sqrt{2rg\frac{\rho_c - \rho_d}{\rho_c}}\,, \quad (38)$$

has been used. This equation is valid for liquid gas droplets with radii >0.5 mm. For smaller droplets the terminal velocity is set to zero.

An equivalent droplet radius can be found from the volume V_d (m^3) of droplets given by

$$V_d = \frac{4}{3}\pi r^3\,, \quad (39)$$

hence the equivalent droplet radius follows from (5),

$$r = \left(\frac{\alpha_d}{\frac{4}{3}\pi n}\right)^{\frac{1}{3}}\,. \quad (40)$$

2.4. Limitations

The following assumptions have been made in the development of the model. First, the droplets are not interacting with each other; that is, there is no merging (splitting) of the droplets to create larger (smaller) particles. Second, in each control volume or in each of the grid nodes in the discrete space, all droplets are assumed to be of the same size. The latter assumption can be argued to represent an average droplet size. However, since the droplets move with increasing velocity with increasing size, the large droplets should enter the neighboring node before the smaller ones.

The mass transfer coefficient in (35) does not incorporate hydrate formation on the droplet/water interface. Hydrate will be formed if the seawater temperature is < ~10°C and at a depth >200–400 m [*Brewer et al.*, 1999]. The thickness of the hydrate layer tends to increase with decreasing temperature, hence decreasing the mass transfer [*Brewer et al.*, 1999; *Warzinski and Holder*, 1999]. There are still large uncertainties in quantifying the decrease in mass transfer caused by hydrate. The study by *Warzinski and Holder* [1999] indicates an order of magnitude reduction in mass transfer at temperature around 5°C, which is the temperature at 700 m off Keahole Point, Hawaii. Another option, used by *Hirai et al.* [1997], is to reduce the concentration difference $C_s - C$ by one half in (37). Recognizing the lack of a consistent parameterization, the mass transfer reduction caused by hydrate formation has been neglected in this study.

Finally, the released heat associated with the dissolution of liquid CO_2 (18) has been neglected in this study. This simplification is based on the relatively small amounts of carbon considered in the numerical experiments reported here. For larger quantities of injected carbon, the effect of heat of dissolution should be included as a source term in the temperature equation (16).

3. Numerical Experiments

3.1. Solution Method and Initialization

There is no equation for the pressure term in the momentum equation for the carrier phase (14). The most frequently used assumption in large-scale ocean models is the hydrostatic approximation, which reduces the vertical momentum equation to a hydrostatic balance equation. This assumption is valid for events on large horizontal scales, but for smaller scales and for events with rapid vertical motion this assumption fails (see, for example, *Marshall et al.* [1997]).

Here we deduce the pressure by using the continuity equation, (13), to find a pressure field that enforces a solenoidal (divergence free) velocity field. For this, a fractional time step method (see, for example, *Ferziger and Perić* [1997]) has been used; first, the momentum equations are solved using the old pressure field, the resulting velocity field is generally not solenoidal and is updated by using a updated pressure field. The latter step involves solving an elliptic problem for the pressure.

For the numerical experiments we have used temperature and salinity profiles from Keahole Point, Hawaii, which has been chosen as a possible site for the first large-scale ocean CO_2 storage field experiment [*Adams et al.*, 1999]. The background velocity field varies as a result of tidal influence and from mesoscale eddies flushing past the island and can reach a speed of 0.1 m s^{-1} [*Adams and Herzog*, 1997,1998].

Table 1. Key Parameters for the Model Experiments.

Name	Background Velocity, m s^{-1}	Droplet Radius, m	Injection Rate, kg CO_2 s^{-1}
Base Case	0.05	0.007	1.0
R01	0.05	0.001	1.0
R12	0.05	0.012	1.0
U00	0.00	0.007	1.0
U10	0.10	0.007	1.0
Ra01	0.05	0.007	0.1

In the numerical experiments presented here, droplet radius, background current, and injection rate vary around a base case characterized with a droplet radius of 7 mm, background current of 0.05 m s^{-1}, and an injection rate of 1 kg CO_2 s^{-1}. Key parameters for the numerical experiments are given in Table 1. The model domain is 254, 62, and 126 m in the along-stream, cross-stream, and vertical directions, respectively. However, in the vanishing background velocity case (U00), the along-stream domain is 127 m. The model equations are solved on an equidistant, staggered grid with 2-m resolution in all directions. All injections occur at 700 m depth.

3.2. Results

Figures 3 and 4 show the time development for the base case experiment in the along-stream vertical cross section through the release point. Figure 3 shows the amount of liquid CO_2 remaining in the droplets per cubic meter, hence showing a picture of the droplet plume. Steady state is achieved after ~10 min, and then the droplets have risen 60 m. The steady state droplet plume stays inclined in the vertical owing to the background current and is continuously feeding CO_2 into the ambient water.

The corresponding pH field is shown in Figure 4. Note how the CO_2 is transported downstream by the background current and downward owing to the increased density of the CO_2-enriched water. The CO_2-enriched water occupies a vertical layer of ~80 m in the base case, starting ~20 m below the release depth. The water with the lowest pH value is, as expected, found close to the injection site.

Terminal or slip velocity increases with increasing droplet size; hence droplets with large radius ascend faster in the water column than smaller droplets, and large droplets also contain more CO_2. Hence large droplets are expected to rise over a longer vertical distance before they, because of dissolution, reach the critical equivalent radius of 0.5 mm, whereafter they follow the background current as a dynamically passive tracer. The CO_2 droplets experience a downward directed force from the descending dense, CO_2-enriched plume water; therefore situations are expected where the droplets may descend.

Figure 5 shows the pH field and the amount of liquid CO_2 per cubic meter remaining in the droplets after 30 min for different droplet release radii. Note how the CO_2-contaminated water and the droplets spread below the injection depth at 700 m when small droplets are injected (Figure 5, top). For initially large droplets, as exemplified in experiment R12 (Figure 5, bottom), the droplet plume rises farther than for the base case experiment and actually exits the model domain at the upper boundary.

When the background velocity increases, the droplet plume inclination increases. Figure 6 is similar to Figure 5, but with vanishing and strong background currents. With no background velocity (Figure 6, top), the droplet plume ascends vertically and the dense plume water sinks to the bottom, where it spreads. The droplet plume and the descending water experience little dilution, leading to a rather large decrease in the pH value. The opposite situation occurs for strong background currents (experiment U10 in Figure 6, bottom). CO_2 is then dissolved into larger water masses, yielding

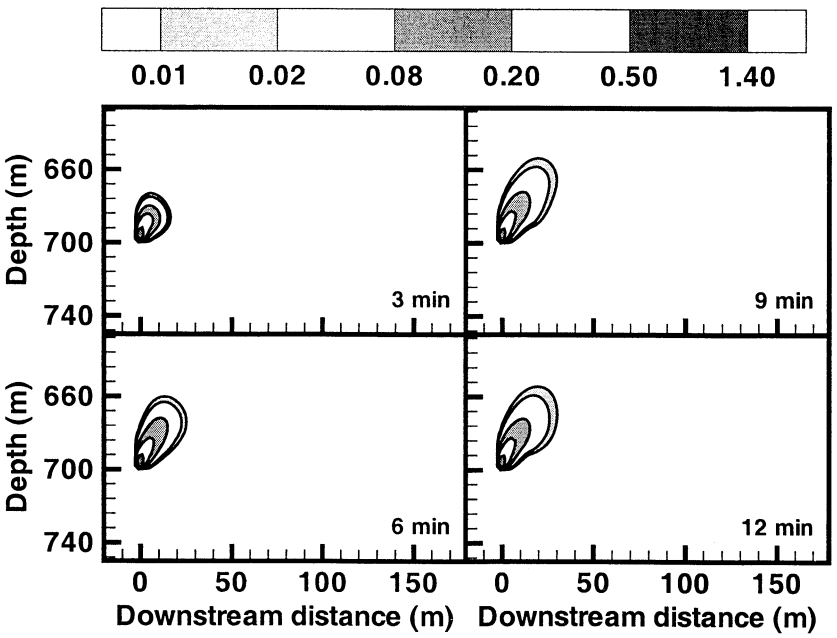

Figure 3. Simulated time evolution of liquid CO_2 in units of kg CO_2 m^{-3} for the base case experiment. Release depth is at 700 m, and a steady state solution is achieved after ~10 min.

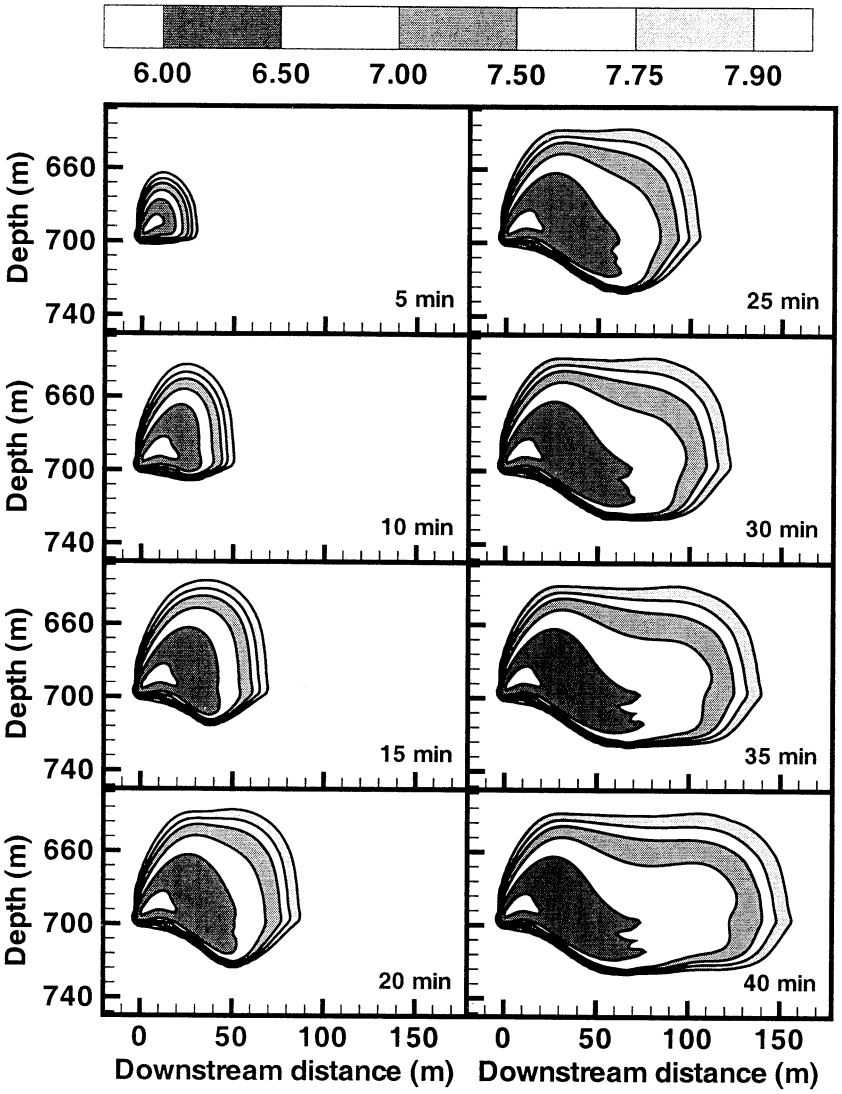

Figure 4. Same as Figure 3, but for the simulated time evolution of the pH field. Background pH value is 7.98.

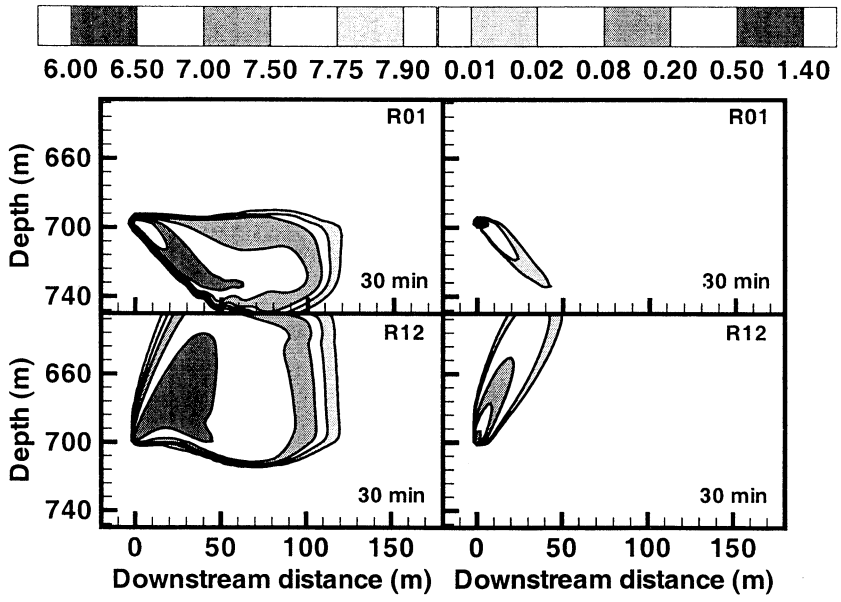

Figure 5. (left) Simulated pH field and (right) the amount of liquid CO_2 (kg CO_2 m^{-3}) in the droplets after 30 min for droplet release radii of (top) 1 mm and (bottom) 12 mm.

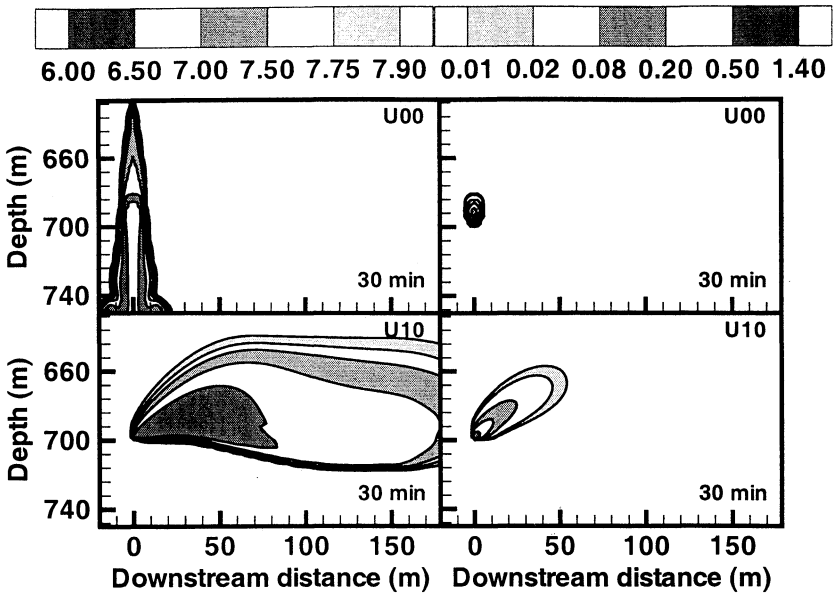

Figure 6. (left) Simulated pH field and (right) the amount of liquid CO_2 (kg CO_2 m^{-3}) in the droplets after 30 min for a droplet release radius of 7 mm and for (top) vanishing and (bottom) 0.1 m s^{-1} background currents.

less acidification and efficient transport of the released CO_2 in the downstream direction.

The last experiment is shown in Figure 7. In this experiment the injection rate of CO_2 is 10% of the base case experiment, so the droplet plume is smaller but still rises 45 m. Notice how the diluted water does not go below the injection depth: In this case the injection rate is too low to generate dense, sinking water.

To illustrate how the CO_2 is distributed in the vertical direction, the amount of dissolved CO_2 as a function of depth has been normalized by the total amount of dissolved inorganic carbon inside a sampling box extending 100 m in the downstream direction, with a sampling volume of 1.28 $\times 10^6$ m^3. Figure 8 shows the vertical distribution of C_T after 30 min. The vertical rising distance of the droplets follows directly from the figure. For base case, U10, and Ra01, the rising distance is ~60 m. In the case with vanishing background velocity, the droplets experience a small positive or even negative buoyancy, leading to a rising distance of only 20 m or so. For the large droplet release case (R12), some of the droplets escape from the model domain, while, as seen earlier, very small droplets (R01) descend in the water column. Hence the initial droplet size is important for determining the vertical distribution of the CO_2 plume.

In order to minimize the influence on marine life, the CO_2-enriched water masses should be kept as diluted as possible. Figure 9 shows the volume of seawater that experiences a reduction in the pH value by more than 1 pH units, using the same sampling box as before (note that the R12 graph is slightly misleading owing to the escape of some of the CO_2 through the upper model boundary). The base case experiment levels off after ~40 min and gives a volume of ~35×10^3 m^3. The high-velocity case levels off earlier (~20 min), and the amount of water with reduced pH is about half that

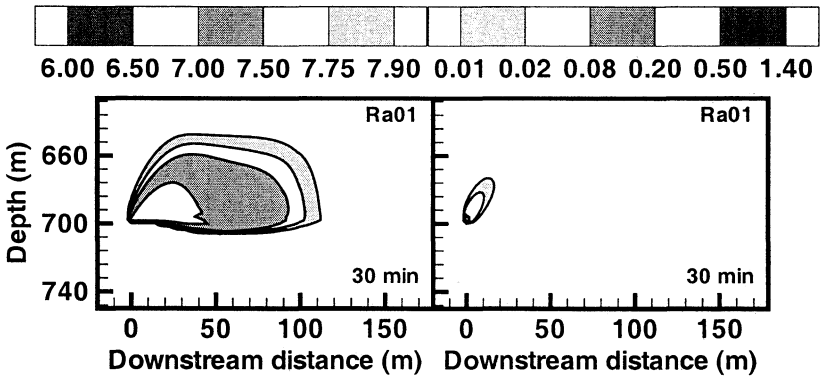

Figure 7. (left) Simulated pH field and (right) the amount of liquid CO_2 (kg CO_2 m^{-3}) in the droplets after 30 min for a droplet release radius of 7 mm and an injection rate of 0.1 kg CO_2 s^{-1}.

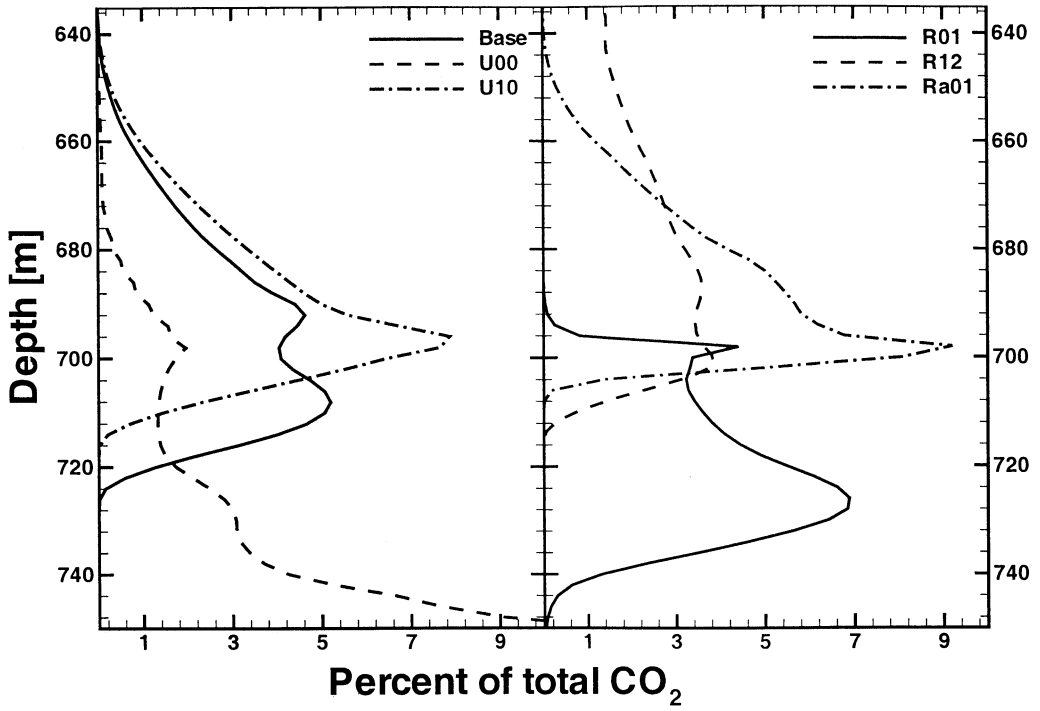

Figure 8. Vertical distribution (in percent of the total dissolved inorganic carbon) as a function of depth for the different experiments (see Table 1). The results have been adjusted for grid spacing so that the depth integral gives 100%. Release depth is at 700 m for all cases.

of the base case. With vanishing background velocity the volume continues to increase as the CO_2-enriched water spreads out on the seafloor. The volume of water masses with reduced pH when the injection rate is 10% of the base case is a factor of ~30 smaller than the corresponding base case volume. The reason for this is that the pH value does not scale linearly with C_T (see Figure 2).

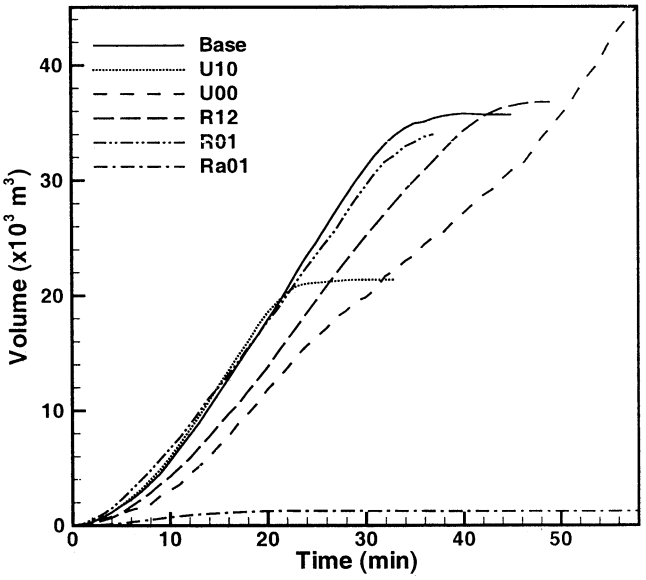

Figure 9. Volume of water ($\times 10^3$ m^3) with more than 1 pH units reduction compared with ambient water as function of time. The different cases are given in Table 1.

4. Discussion

The six numerical experiments discussed in the previous section cover typical parameter values for the pilot large-scale field experiment planned at Keahole Point, Hawaii. The injection rate considered here is small, and, for comparison, the amount of CO_2 injected from a 500 MW gas power plant is a factor of ~65 larger [*Drange et al.*, 1998]. It should be mentioned that the difference between the base case and the Ra01 experiments shows that dissolution of the released CO_2 can be accelerated if the CO_2 is diverted through several ports. In addition, low injection rates narrow the CO_2-exposed layer owing to the small density increase of the plume water.

It is further shown that strong background currents decrease the vertical extent of CO_2-containing water, and downward movement of this water is absent or moderate owing to entrainment of ambient water. In the case of vanishing background currents the released CO_2 may reach the seafloor, with possible impact on the benthic boundary layer biota and sediments. The droplet release radius is a key parameter in governing the vertical distribution of the droplets and hence the extent of the vertical layer that is influenced by dissolved CO_2. For instance, very small particles (radius of 1 mm) lead to downward transport of the released

CO_2, whereas a rising distance of >100 m is possible for droplets with initial radius >10 mm.

Two of the main considerations for evaluating CO_2 injection in the ocean as a mitigation strategy is the residence time of the released CO_2 and the biological impact from reduced pH close to the injection site. The upper turbulent mixed layer of the ocean should be avoided, since partial outgassing of the released carbon is expected if the CO_2 enters this layer (H. Drange et al., manuscript in preparation, 2000). In this respect it is preferable to generate high concentration CO_2 plume water or simply dissolve the CO_2 at the level at which it is introduced, leading to sinking plumes of CO_2-enriched water. The drawback of generating high CO_2 concentration water is the increased acidification of the plume fluid. Obviously, the two considerations must be balanced for a given injection site, and the result will depend on the ocean dynamics and the marine fauna in the vicinity of the site.

5. Conclusion

CO_2 injection in the ocean by droplet release is a possible option for accelerating the natural net flux of carbon from the atmosphere to the ocean. Ocean storage of CO_2 is successful only if outgassing of the released CO_2 is small on a century timescale and if the environmental effects are negligible. The present study indicates that the initial size of the CO_2 droplets in combination with the flux of carbon through each of the release ports may be adjusted so that environmental effects can be minimized. It is of paramount importance to perform effect studies in order to assess the stress that marine organisms will experience in the vicinity of a given release site. Also, the cumulative effect on the marine biota caused by a multiple of large-scale release sites should be considered. Finally, the influence of hydrate formation on the droplet surface is another subject that needs further attention.

Acknowledgments. This study has been supported by the Norwegian Research Council through the KLIMATEK programme and by the G. C. Rieber Climate Institute at NERSC. Thanks to Eric Adams of the Civil and Environmental Laboratory, Massachusetts Institute of Technology (MIT), for his hospitality during G.A.'s visit to Boston and Brian Cournse, MIT, for providing the profiles for Keahole Point. We also thank Ola M. Johannessen, NERSC, and Finn Thorkildsen, Statistics Norway, for valuable input during this study.

References

Adams, E., and H. Herzog, Scoping and site selection study for an ocean CO_2 disposal field experiment, *technical report*, Mass. Inst. of Technol., Cambridge, 1997.

Adams, E., and H. Herzog, Site selection study for an ocean CO_2 disposal field experiment, *technical report* , Mass. Inst. of Technol., Cambridge, 1998.

Adams, E., D. Golumb, X. Y. Zhang, and H. J. Herzog, Confined release of CO_2 into shallow seawater, in *Direct Ocean Disposal of Carbon Dioxide*, edited by N. Handa, and T. Ohsumi, pp. 153–164, Terra Sci., Tokyo, 1995.

Adams, E., M. Akai, L. Golmen, P. M. Haugan, H. Herzog, S. Masuda, S. Masutani, T. Ohsumi, and C. C. Wong, An international experiment on CO_2 ocean sequestration, in *Greenhouse Gas Control Technologies*, edited by P. Riemer, B. Eliasson, and A. Wokaun, pp. 293–298, Elsevier Sci., New York, 1999.

Alendal, G., Implementing and testing of different gravity current models with application to oceanic and man-made currents., Ph.D. thesis, Univ. of Bergen, Bergen, Norway, November 1996.

Alendal, G., H. Drange, and P. M. Haugan, Modelling of deep-sea gravity currents using an integrated plume model, in *The Polar Oceans and Their Role in Shaping the Global Environment: The Nansen Centennial Volume, Geophys. Monogr. Ser. vol-85,* edited by O. M. Johannessen, R. D. Muench, and J. E. Overland, pp. 237–246, AGU, Washington, D. C., 1994.

Auerbach, D. I., J. A. Caulfield, E. Adams, and H. J. Herzog, Impacts of ocean CO_2 disposal on marine life: A toxicological assessment integrating constant–concentration laboratory data with variable–concentration field exposure, *Environ. Model. Assess., 2*, 333–343, 1997.

Bacastow, R., and G. R. Stegen, Estimating the potential for CO_2 sequestration in the ocean using a carbon cycle model, *Oceanus, 3*, 1654–1657, 1991.

Bradshaw, A., The effect of carbon dioxide on the specific volume of seawater, *Limnol. Oceanogr., 18*, 95–105, 1973.

Brewer, P. G., G. Friederich, E. T. Peltzer, and F. M. Orr Jr., Direct experiments on the ocean disposal of fossil fuel CO_2, *Science, 284*, 943–945, 1999.

Broecker, W. S., and T.-H. Peng, *Tracers in the Sea*, Lamont-Doherty Earth Obs., Palisades, N. Y., 1982.

Caulfield, J. A., E. Adams, D. I. Auerbach, and H. J. Herzog, Impacts of ocean CO_2 disposal on marine life: Probabilistic plume exposure model used with a time–varying dose response analysis, *Environ. Model. Assess., 2*, 345–353, 1997.

Clift, R., J. Grace, and M. Weber, *Bubbles, Drops, and Particles*, Academic, San Diego, Calif., 1978.

Crowe, C., M. Sommerfeld, and Y. Tsuji, *Multiphase Flows with Droplets and Particles*, CRC Press, Boca Raton, Fla., 1998.

Cussler, E. L., *Diffusion. Mass Transfer in Fluid Systems*, Cambridge Univ. Press, New York, 1984.

Drange, H., and P. M. Haugan, A feasibility study of dissolution and sequestration of CO_2 in the ocean, *Tech. Rep.* 54, Nansen Environ. and Remote Sens. Cent., Bergen, Norway, 1992a.

Drange, H., and P. M. Haugan, Carbon dioxide sequestration in the ocean: The possibility of injection in shallow water, *Energy Convers. Manage., 33*, 697–704, 1992b.

Drange, H., G. Alendal, and P. M. Haugan, A bottom gravity current model for CO_2-enriched seawater, *Energy Convers. Manage., 34*, 1065–1072, 1993.

Drange, H., G. Alendal, F. Thorkildsen, and O. M. Johannessen, Geophysical/economical feasibility study of ocean disposal of CO_2 at Haltenbanken, *Tech. Rep.* 138, Nansen Environ. and Remote Sens. Cent., Bergen, Norway, 1998.

Ely, J. F., W. M. Haynes, and B. C. Bain, Isochoric (p, V_m, T) measurements on CO_2 and on ($0.982CO_2$ + $0.01N_2$) from 250 to 330 K at pressures to 35 MPa, *J. Chem. Thermodyn., 21*, 879–894, 1989.

Ferziger, J. H., and M. Perić, *Computational Methods for Fluid Dynamics*, Springer–Verlag, New York, 1997.

Golomb, D. S., S. G. Zemba, J. W. Dacey, and A. F. Michaels, The fate of CO_2 sequestered in the deep ocean, *Energy Convers. Manage., 33*, 675–683, 1992.

Haugan, P. M., and H. Drange, Sequestration of CO_2 in the deep ocean by shallow injection, *Nature*, *357*, 318–320, 1992.

Herzog, H., D. Golomb, and S. Zemba, Feasibility, modelling and economics of sequestering power plant CO_2 emissions in the deep ocean, *Environ. Prog.*, *10*, 64–74, 1991.

Hirai, S., K. Okazaki, Y. Tabe, and K. Hijikata, Numerical simulation for dissolution of liquid CO_2 droplets covered by clathrate film in intermediate depth of ocean, *Energy Convers. Manage.*, *38*, S313–S318, 1997.

Hoffert, M. I., Y.-C. Wey, A. J. Callegari, and W. S. Broecker, Atmospheric response to deep-sea injections of fossil-fuel carbon dioxide, *Clim. Change*, *2*, 53–68, 1979.

Liro, C. R., E. E. Adams, and H. J. Herzog, Modeling the release of CO_2 in the deep ocean, *Energy Convers. Manage.*, *33*, 667–674, 1992.

Maier-Reimer, E., Carbonate buffering of anthropogenic CO_2, in *Strategies for Future Climate Research*, edited by M. Latif, pp. 319–339, Max-Planck-Inst. für Meteorol., Hamburg, Germany, 1991.

Marchetti, C., On geoengineering and the CO_2 problem, *Clim. Change*, *1*, 59–68, 1977.

Marshall, J., C. Hill, L. Perelman, and A. Adcroft, Hydrostatic, quasi–hydrostatic, and nonhydrostatic ocean modeling, *J. Geophys. Res.*, *102*(C3), 5733–5752, 1997.

McComb, W. D., *The Physics of Fluid Turbulence*, Clarendon Press, Oxford, England, 1990.

Nakashiki, N., T. Ohsumi, and K. Shitashima, Sequestering of CO_2 in a deep-ocean. Fall velocity and dissolution rate of solid CO_2 in the ocean, *Tech. Rep.* EU91003, ABIKO Res. Lab., Abiko, Japan, 1991.

Ohsumi, T., Prediction of solute carbon dioxide behavior around a liquid carbon dioxide pool on deep ocean basins, *Energy Convers. Manage.*, *34*, 1059–1064, 1993.

Saji, A., H. Yoshida, M. Sakaii, T. Tanii, T. Kamata, and H. Kitamura, Fixation of carbon by clathrate-hydrate, *Energy Convers. Manage.*, *33*, 643–649, 1992.

Schimel, D., D. Alves, I. Enting, M. Heimann, F. Joos, D. Raynaud, and T. Wigley, Radiative forcing of climate change. CO_2 and the carbon cycle, in *Climate Change 1995: The Science of Climate Change. Contribution of Working Group I to the Second Assessment Report of the Intergovernmental Panel on Climate Change*, edited by J. T. Houghton et al., pp. 76–86, Cambridge Univ. Press, New York, 1996.

Shindo, Y., P. Lund, Y. Fujioka, and H. Komiyama, Kinetics of formation of CO_2 hydrate, *Energy Convers. Manage.*, *34*, 1073–1079, 1993.

Stegen, G. R., K. H. Cole, and R. Bacastow, The influence of discharge depth and location on the sequestration of carbon dioxide, *Energy Convers. Manage.*, *34*, 857–864, 1993.

Stumm, W., and J. J. Morgan, *Aquatic Chemistry*, 2nd ed., Wiley-Interscience, New York, 1981.

Sundquist, E. T., Geologic analogs: Their value and limitation in carbon dioxide research, in *The Changing Carbon Cycle. A Global Analysis*, edited by J. R. Trabalka et al., pp. 371–402, Springer-Verlag, New York, 1986.

Thorkildsen, F., and G. Alendal, LES study of flow around a CO_2-droplet plume in the ocean, *Energy Convers. Manage.*, *38*, S361–S366, 1997.

Thorkildsen, F., and P. Haugan, Numerical model for plumes of dissolving CO_2 droplets in seawater, *Tech. Rep.* 78, Nansen Environ. and Remote Sens. Cent., Bergen, Norway, 1993.

Thorkildsen, F., G. Alendal, and P. Haugan, Modelling of CO_2 droplet plumes, *Tech. Rep.* 96, Nansen Environ. and Remote Sens. Cent., Bergen, Norway, 1994.

UNESCO, Tenth report of the joint panel on oceanographic tables and standards, UNESCO Tech. Pap. Mar. Sci., 36, 1981.

Warzinski, R. P., and G. D. Holder, Ocean storage of CO_2: Experimental observations of clathrate hydrates in seawater, in *Greenhouse Gas Control Technologies*, edited by P. Riemer, B. Eliasson, and A. Wokaun, pp. 1061–1063, Elsevier Sci., New York, 1999.

Wilson, T. R. S., The deep ocean disposal of carbon dioxide, *Energy Convers. Manage.*, *33*, 627–633, 1992.

Yakhot, V., and S. A. Orszag, Renormalization group analysis of turbulence, I, Basic Theory, *J. Sci. Comput.*, *1*(1), 3–51, 1986.

G. Alendal and H. Drange, Nansen Environmental and Remote Sensing Center, Edvard Griegsvei 3a, N–5059 Bergen, Norway. (Guttorm.Alendal@nrsc.no; Helge.Drange@nrsc.no)

(Received March 12, 1999; revised April 4, 2000; accepted August 23, 2000.)